Fusion Technology

ISSN: 0748-1896 (Print) (Online) Journal homepage: http://www.tandfonline.com/loi/ufst19

TJ-II Project: A Flexible Heliac Stellarator

Carlos Alejaldre, Jose Javier Alonso Gozalo, Jose Botija Perez, Francisco Castejón Magaña, Jose Ramon Cepero Diaz, Jose Guasp Perez, A. Lopez-Fraguas, Luis García, Vladimir I. Krivenski, R. Martín, A. P. Navarro, Angel Perea, Antonio Rodriguez-Yunta, Mario Sorolla Ayza & Antonio Varias

To cite this article: Carlos Alejaldre, Jose Javier Alonso Gozalo, Jose Botija Perez, Francisco Castejón Magaña, Jose Ramon Cepero Diaz, Jose Guasp Perez, A. Lopez-Fraguas, Luis García, Vladimir I. Krivenski, R. Martín, A. P. Navarro, Angel Perea, Antonio Rodriguez-Yunta, Mario Sorolla Ayza & Antonio Varias (1990) TJ-II Project: A Flexible Heliac Stellarator, Fusion Technology, 17:1, 131-139, DOI: 10.13182/FST17-131-139

To link to this article: https://doi.org/10.13182/FST17-131-139

Published online: 09 May 2017.

TJ-II PROJECT: A FLEXIBLE HELIAC STELLARATOR

STELLARATOR SYSTEMS

KEYWORDS: *TJ-II, stellarator, Heliac*

CARLOS ALEJALDRE, JOSE JAVIER ALONSO GOZALO, JOSE BOTIJA PEREZ, FRANCISCO CASTEJÓN MAGAÑA, JOSE RAMON CEPERO DIAZ, JOSE GUASP PEREZ, A. LOPEZ-FRAGUAS, LUIS GARCÍA,* VLADIMIR I. KRIVENSKI, R. MARTÍN, A. P. NAVARRO, ANGEL PEREA, ANTONIO RODRIGUEZ-YUNTA, MARIO SOROLLA AYZA, and ANTONIO VARIAS *Asociación EURATOM/CIEMAT para Fusión 28040 Madrid, Spain*

Received April 10, 1989
Accepted for Publication August 8, 1989

The TJ-II device is a medium-size (R_0 = 1.5 m, $\langle a_p \rangle$ = 0.2 to 0.25 m, B_0 = 1 T) helical-axis stellarator to be built at the CIEMAT site in Madrid. Its main characteristics are (a) potential for high-beta operation; (b) flexibility, i.e., its rotational transform can be varied over a wide range and its shear to some extent; and (c) bean-shaped plasma cross section. The latest understanding of TJ-II physics in the fields of electron cyclotron resonance heating, transport, and magnetohydrodynamics, and the engineering solutions introduced in its final design are discussed.

INTRODUCTION

Helical magnetic axis devices have a potential for high beta that makes them especially interesting as fusion reactor candidates. To explore this capability, the TJ-II experiment was designed as a device with enough flexibility to cover a wide range of rotational transform values, to determine the most adequate operating conditions in a first experimental step with up to 600 kW of electron cyclotron resonance heating (ECRH) devoted to equilibrium, stability, and transport studies. The engineering design has also been made compatible with higher power deposition in the vacuum chamber so that neutral beam injection will be possible in a second experimental step, with additional powers up to 4 MW, to study the finite-beta effects in the results of the first experimental program and the limits in beta for this configuration.

*Current address: Universidad Complutense, Madrid, Spain.

DESCRIPTION

The TJ-II configuration, shown in Fig. 1, consists of 32 toroidal field (TF) coils whose centers follow a toroidal helix of major radius R_0 = 1.5 m, minor radius r_{sw} = 0.28 m, and pitch law $\theta = -4\Phi$, where θ and Φ are the usual poloidal and toroidal angles. The central conductors, called the hard core, are made of two components, a circular coil centered at the major axis (1.5 m) and a helical winding wrapped around the circular coil following the same winding law as the TF coils (see separate detail in Fig. 1). Separately controllable currents in the hard core windings give the device its unique flexibility[1,2] and differentiate it from the original heliac design.[3,4] Two circular vertical field (VF) coils complete the coil configuration. These coils add a vertical magnetic field of ≈5% of the TF strength and are used to control the position of the magnetic axis. The magnetic surfaces are bean-shaped for the entire operational space, also shown in Fig. 1. Table I summarizes the main parameters of the TJ-II device.

Plasma Heating

In the first stage, plasma breakdown and heating will be produced by an ECRH system. Preliminary experiments will be done with a 200-kW, 28-GHz gyrotron. Due to the density-dependent cutoffs in the wave propagation frequency and to obtain more relevant plasmas in the TJ-II, an ECRH system based on two gyrotrons, each 200 kW working at 53.2 GHz, will be provided.

To account for the particularly difficult TJ-II geometry, the three-dimensional ray-tracing RAYS code[5] developed at Oak Ridge National Laboratory has been adapted to the geometry of TJ-II, and a new absorption module has been introduced that permits

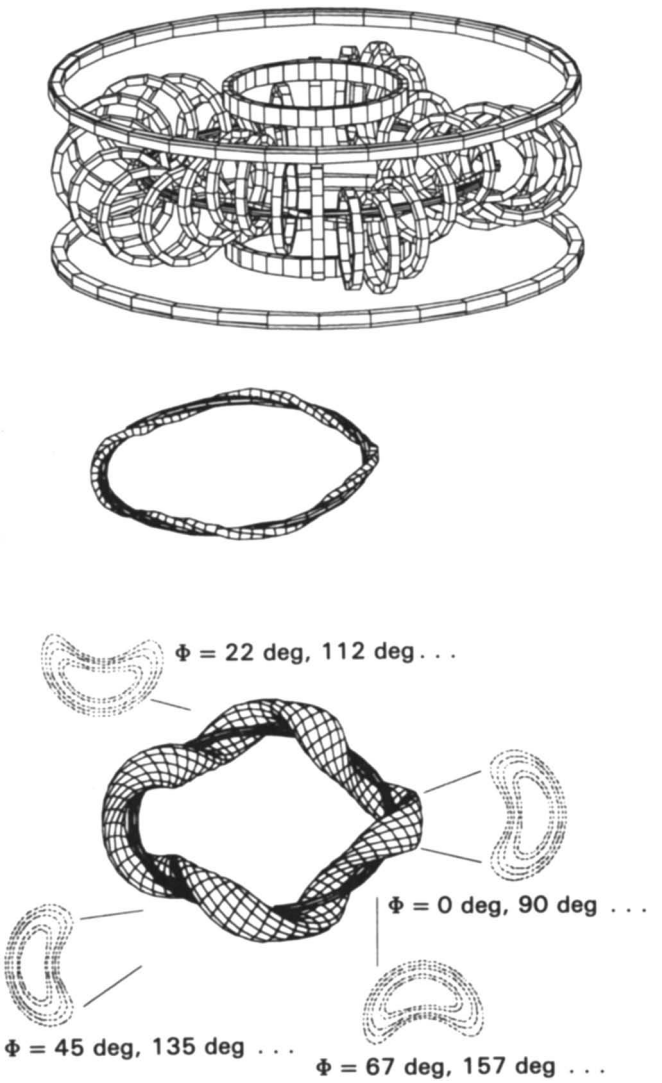

Fig. 1. TJ-II coil configuration.

calculation of the power absorption when a non-Maxwellian electron distribution is present.[6] A study using RAYS, taking into consideration the limitations of the actual vacuum chamber for access to the plasma, has been conducted to obtain the optimum position of ray launching to maximize the power deposition and control the temperature profile. Figure 2 shows ray trajectories for X-mode propagation in the second harmonic assuming a bunch of nine rays in a 5-mm launching beam at toroidal position $\Phi = 17$ deg. The figure also shows the access ports to the vacuum chamber, the flux surfaces, and the resonance layer. Plasma conditions assumed in this study are $n_e(0) = 1.5 \times 10^{19}$ m^{-3} and $T_e(0) = 1$ keV. The power absorbed by the plasma in one pass has maximum values of the order of 40% for O-mode propagation at the first harmonic and in excess of 99% for X-mode propagation at the second harmonic.

TABLE I

TJ-II Main Parameters

Design Parameters	
Major radius (m)	1.5
Average magnetic field (T)	1
Number of periods	4
Number of TF coils	32
TF coil radius (m)	0.425
TF coil swing (m)	0.2825
TF coil current (nominal 1 T) (kA)	234
$l = 1$ helical coil swing (m)	0.07
VF coil radius (m)	2.25
VF coil height (m)	±0.75
Maximum circular coil current, I_{cc} (kA)	−280
Maximum helical coil current, I_{hc} (kA)	−200
Maximum VF current (kA)	200
Calculated Ranges	
Range for rotational transform at magnetic axis	0.96 to 2.5
Range of plasma average radius (m)	0.10 to 0.25
Shear range (%)	−1 to +10
Magnetic well depth range (%)	0 to 6

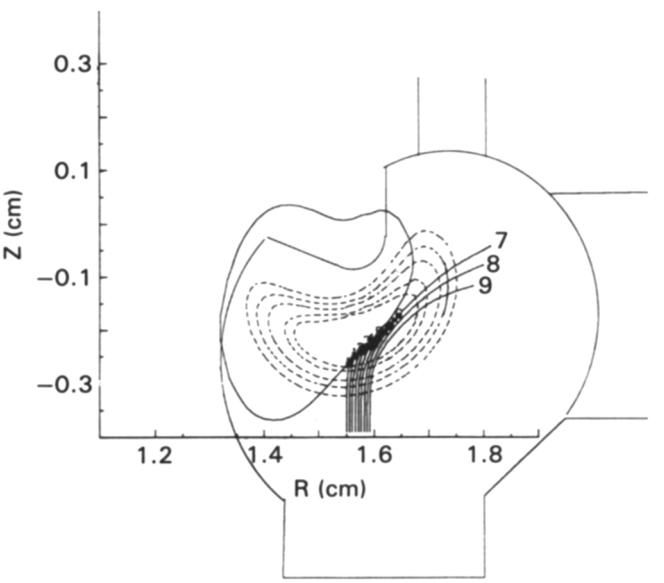

Fig. 2. Microwave trajectories for X-mode propagation in the second harmonic.

Since quasi-linear effects can play a major role during ECRH through a deformation of the electron distribution function that in turn can change the absorption process, we calculated the distortion in the electron distribution function $f(u_\perp, u_\parallel, t)$, by solving the following kinetic equation[7]:

$$\frac{\partial f}{\partial \tau} = \frac{1}{u_\perp}\left(\frac{\omega_c}{\omega}\frac{\partial}{\partial u_\perp} + \frac{u_\perp}{\mu^{1/2}}\frac{\partial}{\partial u_\parallel} n_\parallel\right) \times u_\perp D_{cy}\left(\frac{\omega_c}{\omega}\frac{\partial}{\partial u_\perp} + \frac{n_\parallel u_\perp}{u^{1/2}}\frac{\partial}{\partial u_\parallel}\right) f + \left(\frac{\partial f}{\partial \tau}\right)_{coll} ,$$

where

$\mu = mc^2/kT_e$

τ = time normalized to the collision frequency

D_{cy} = diffusion coefficient due to the applied wave

ω, ω_c = incident wave and the cyclotron frequencies, respectively

$n_\parallel$ = parallel component of the plasma refraction index

$u_\parallel, u_\perp$ = normalized parallel and normal components of the particle momentum.

The strong absorption at the second harmonic induces strong quasi-linear effects that degrade power absorption to ~90% at $\tau = 1.8$ and 30% when $\tau \approx 14$. Figure 3 shows the contours of constant $-\ln f$ for $\tau \approx 10$. It demonstrates the strong deformation that the electron distribution function suffers when deposition occurs at the axis with perpendicular illumination. The dotted lines delineate the trapped particle region. Work is continuing to determine the optimum incidence angle to minimize quasi-linear effects.

Transport

By modulating the TF coil currents, we should be able to modify the magnetic field ripple at the magnetic axis and therefore optimize the transport properties in TJ-II. One technique is to use independent current feed to each TF coil. Studies in this line show that TF coils can be grouped in five sets to minimize ripple, which would considerably increase the power supply costs and the bus compensation requirements. An easier and less expensive method to minimize the magnetic field ripple at the axis is to spatially displace the TF coil locations from the equally toroidal arrangement, in accordance with the following law:

$$\Delta\Phi_i = 2\pi/N * 1/[1 + \alpha \cos M(\Phi_i + \Delta\Phi_i/2)] ,$$

where α is the free parameter to minimize the ripple.

Figure 4 shows the harmonic content of the magnetic field magnitude as a function of the normalized magnetic flux $s = \Psi/\Psi_{max}$ for both before and after the toroidal displacement of the coils. It can be seen how the harmonic content of the field diminishes globally; in particular, the corner ripple term (0,4), due to the "square" shape of the TJ-II, almost disappears.

Using the Monte Carlo code described in Refs. 8 and 9, we have calculated the thermal conductivity and diffusion transport coefficients for both electrons and ions in a TJ-II configuration with $\iota(0) = 1.52$ and $\langle\beta\rangle \approx 1\%$. We estimate the value of the ambipolar electric field and the resulting confinement time for several heating situations assuming parabolic radial profiles.

Figure 5 shows the normalized diffusion coefficient D^* ($= D/D_{\text{plateau tokamak}}$) as a function of the normalized frequency ν^* ($= \pi R_0 \nu/\iota v_t$) for the magnetic surface located at $\langle r\rangle = a_p/2$ and several values of the radial electric field. The solid line corresponds, for comparison purposes, to the diffusion coefficient for the equivalent tokamak, with the same rotational transform. The influence of a radial electric field on transport can be clearly seen in the figure. For strong enough electric fields, the $1/\nu$ regime can disappear, and particles go directly from the plateau to the $\nu^{1/2}$

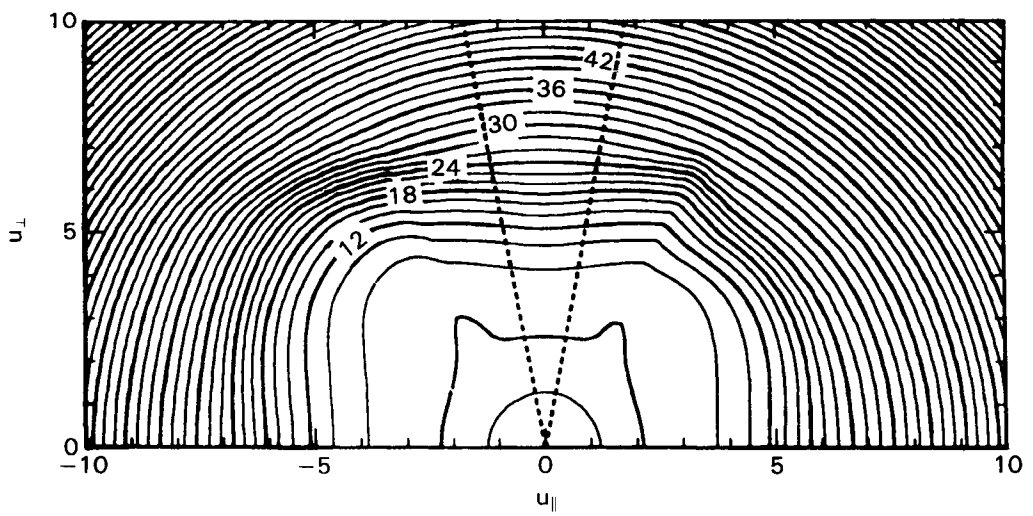

Fig. 3. ECRH effect on electron velocity distribution function.

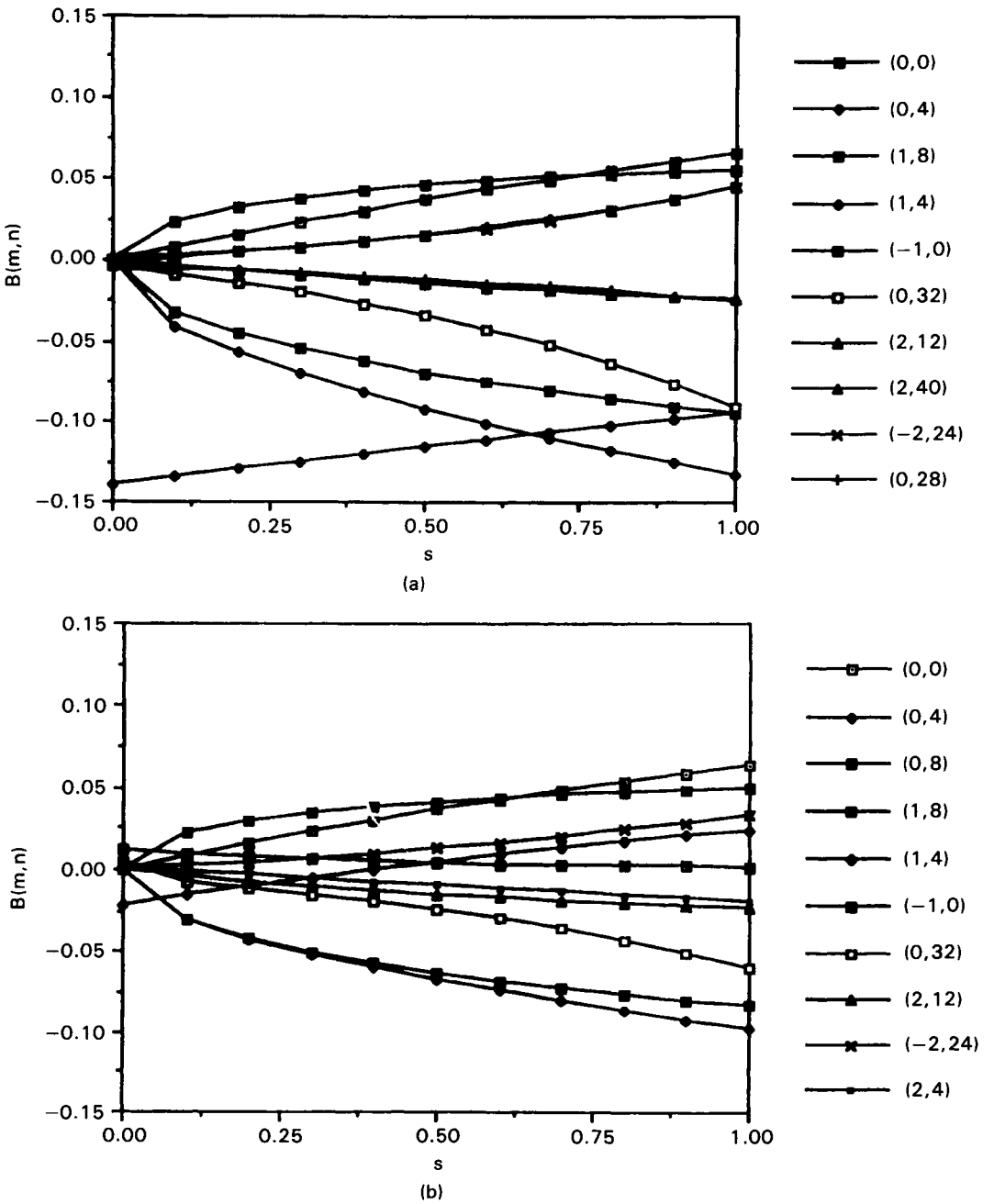

Fig. 4. Fourier components of the magnetic field (a) before and (b) after spatial modulation of the TF coil toroidal locations.

regime. Table II shows the confinement times for the electric fields obtained from the ambipolarity condition $\Gamma_i(\psi) = \Gamma_e(\psi)$.

Stability

The high degree of flexibility in TJ-II makes it a very attractive device to study the stability properties of helical-axis plasmas with a broad range of rotational transform and magnetic well values. This flexibility will permit experimentally exploring regimes with average stability beta limits ranging from near zero to 6% in an almost continuous manner.[10]

We have studied four configurations with the same rotational transform, but different magnetic wells. The parameters for the configurations are summarized in Table III. Figure 6 shows the flux surfaces for the four configurations at the toroidal angle $\Phi = 0$ deg. Fixed boundary equilibria for the four configurations were obtained using the three-dimensional equilibrium code

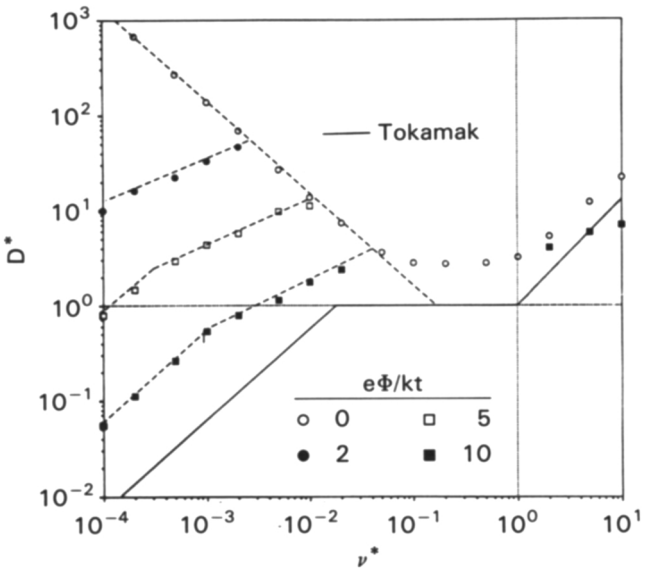

Fig. 5. Normalized diffusion coefficient for the $a_p/2$ surface and several values of the radial electric field.

TABLE II

TJ-II Predicted Confinement Times*

$\iota(0)$	$e\Phi/KT_e$	τ_p[a] (ms)	τ_{ee}[b] (ms)	τ_{ei}[b] (ms)	τ_e[c] (ms)
Without Coil Modulation					
1.51	+1.8	7.6	2.2	4.5	2.5
With Coil Modulation					
2.19	+1.7	13.5	3.8	7.5	4.3
1.52	+1.6	13.8	3.9	7.7	4.4
1.18	+1.3	15.6	4.5	8.7	5.0

*For $n_e = 1.65 \times 10^{19}$ m^{-3}, $T_e = 620$ eV, and $T_i = 170$ eV.
[a]τ_p = particle confinement time.
[b]τ_{ee}, τ_{ei} = electron and ion energy confinement times.
[c]τ_e = global energy confinement time.

TABLE III

TJ-II Configurations Used in Stability Studies

Configuration	$\iota(0)/M$	$-I_{cc}$ (kA)	$-I_{hc}$ (kA)	Magnetic Well (%)
A1	0.36	65	55	1
A2 (standard)	0.36	105	82.5	2
A3	0.36	219	95	3
A4	0.36	280	92	4

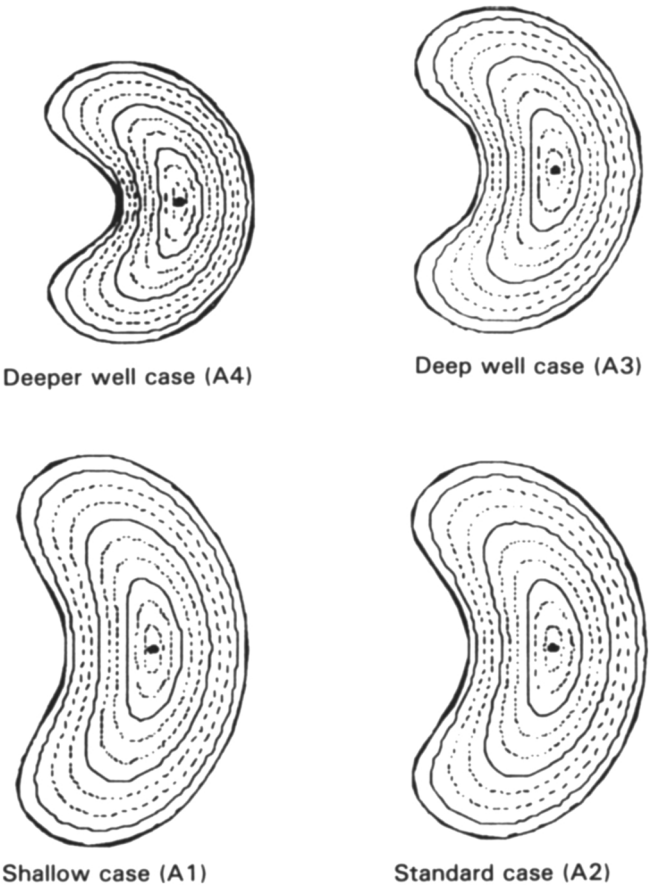

Fig. 6. The four vacuum configurations used in the stability studies.

VMEC (Ref. 11) with a radial mesh of 31 points. We needed 138 Fourier amplitudes to satisfactorily characterize the boundary of the confinement region. We considered a sequence of zero-current equilibria with a pressure profile $p \propto (1 - \psi)$, where ψ is the normalized toroidal flux.

Figure 7 shows the result of applying a three-dimensional Mercier criterion to the four configurations at a fixed radius. A larger radius was chosen because plasma stability decreases for increasing radial position. An equilibrium is considered stable when the criterion is positive. We found that the configuration with a shallow well depth (A1) is unstable to Mercier modes even at small beta values but when the vacuum well becomes deeper, its stability increases until the beta limit exceeds 6% for the extreme case (A4).

A second set of configurations with a rotational transform per period of $\iota(0)/M \approx 0.3$ and slightly different vacuum magnetic wells (see Table IV) was also studied. The qualitative behavior of these configurations is quite different from the previous case. Figure 8 shows the result of applying a three-dimensional Mercier criterion to a set of zero-current equilibria obtained

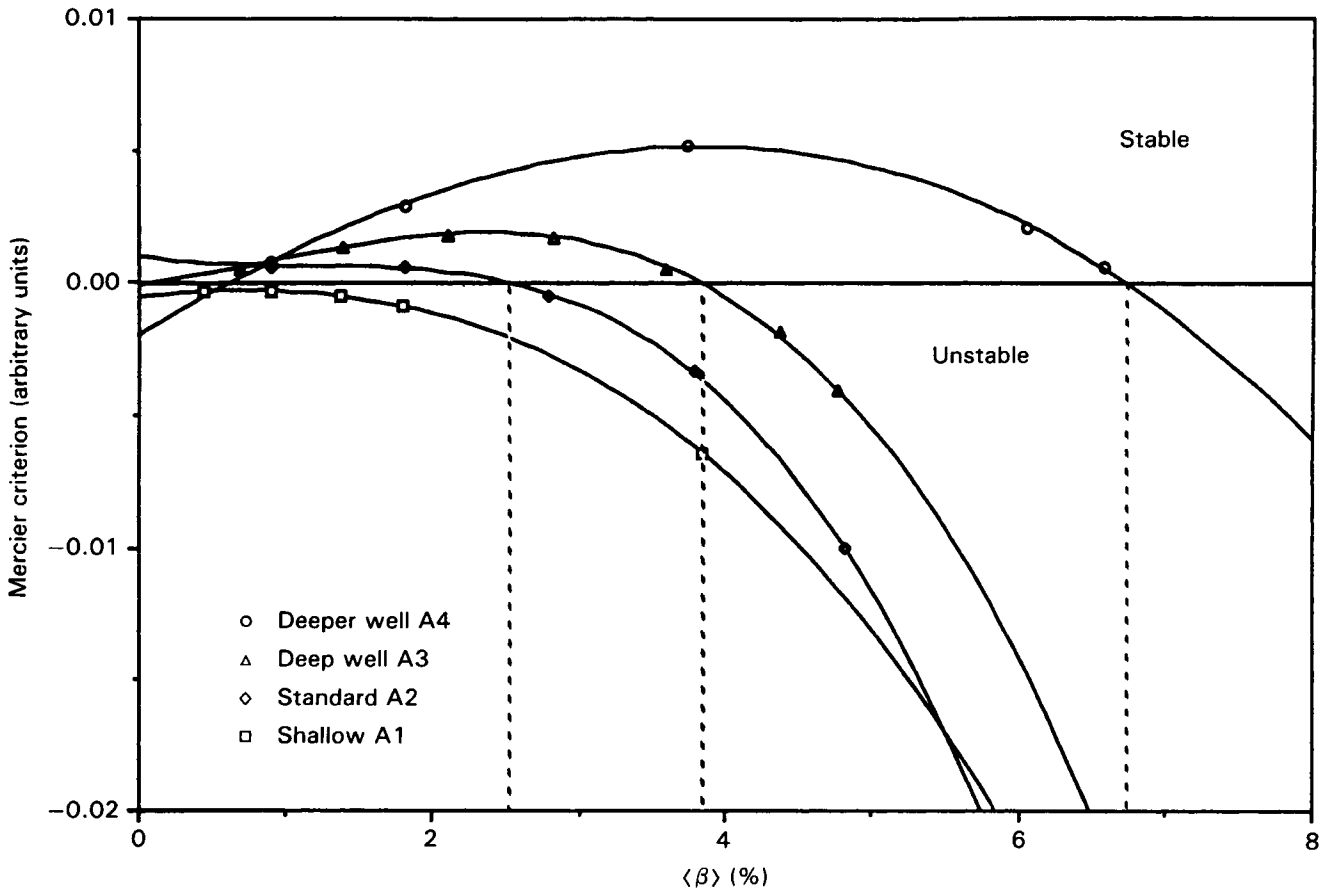

Fig. 7. The Mercier stability criterion versus $\langle\beta\rangle$ at a fixed normalized radius ($r/a_p = 0.96$) for the four configurations in Fig. 6.

TABLE IV

TJ-II Configurations for Second Stability Regime Study

Configuration	$\iota(0)/M$	$-I_c$ (kA)	$-I_h$ (kA)	Magnetic Well (%)
B1	0.30	163	39	1.5
B2	0.30	82	42	1.6

for $\langle\beta\rangle$ increasing from 0 to 6%. Self-stabilization effects typical of a second stability regime are clearly seen for values of $\langle\beta\rangle \geq 5\%$. Figure 9 summarizes the results of a similar study for configuration B2, which gives an even more positive picture of its stability properties: It is stable to Mercier modes over the whole radius and again at $\langle\beta\rangle \approx 4\%$, within the available power in the last stage of the TJ-II experimental program, and shows a marked self-stabilization behavior.

Work is under way to study configurations with deeper magnetic wells, higher effective aspect ratios, and high rotational transform [$\iota(0)/M \approx 0.6$].

ENGINEERING STUDIES

A detailed design for TJ-II is under way at Ansaldo Componenti with participation of engineers from EURATOM/CIEMAT and ENEA-Frascati. Solutions for the main components of this device has been found and are described below.

Vacuum Chamber

The chosen solution has the hard core conductors outside the vacuum chamber with a noticeable relaxation in the feasibility requirements for these coils. This is possible by making the chamber almost circular with a helical indentation to accommodate the hard core coils. Even with this restriction, it is possible to build the chamber by octants. These octants will be joined by flanges that will help to achieve the geometrical accuracy required for this device. Figure 10 shows an octant of the vacuum chamber. Special protection for energy and particle deposition has been designed: There is a toroidal shield for the thinnest part of the chamber and protection all along the hard core position and at nine toroidal locations, covering the welding between adjacent sectors.

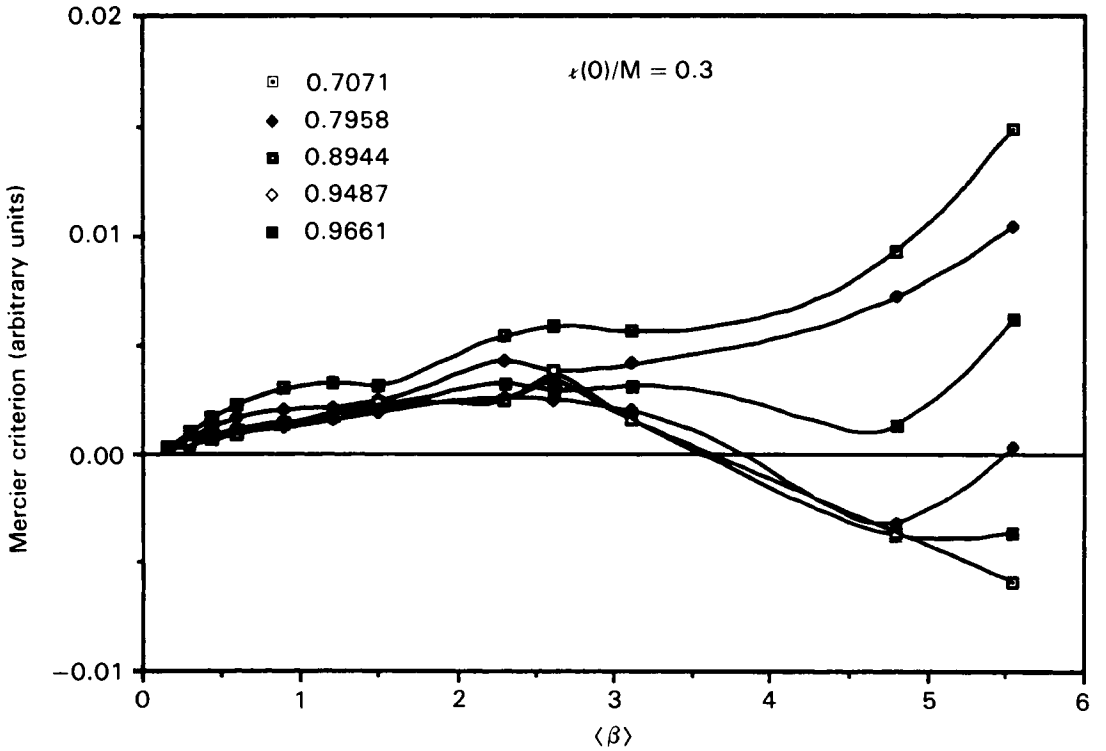

Fig. 8. The Mercier stability criterion versus $\langle\beta\rangle$ at several normalized radii for configuration B1.

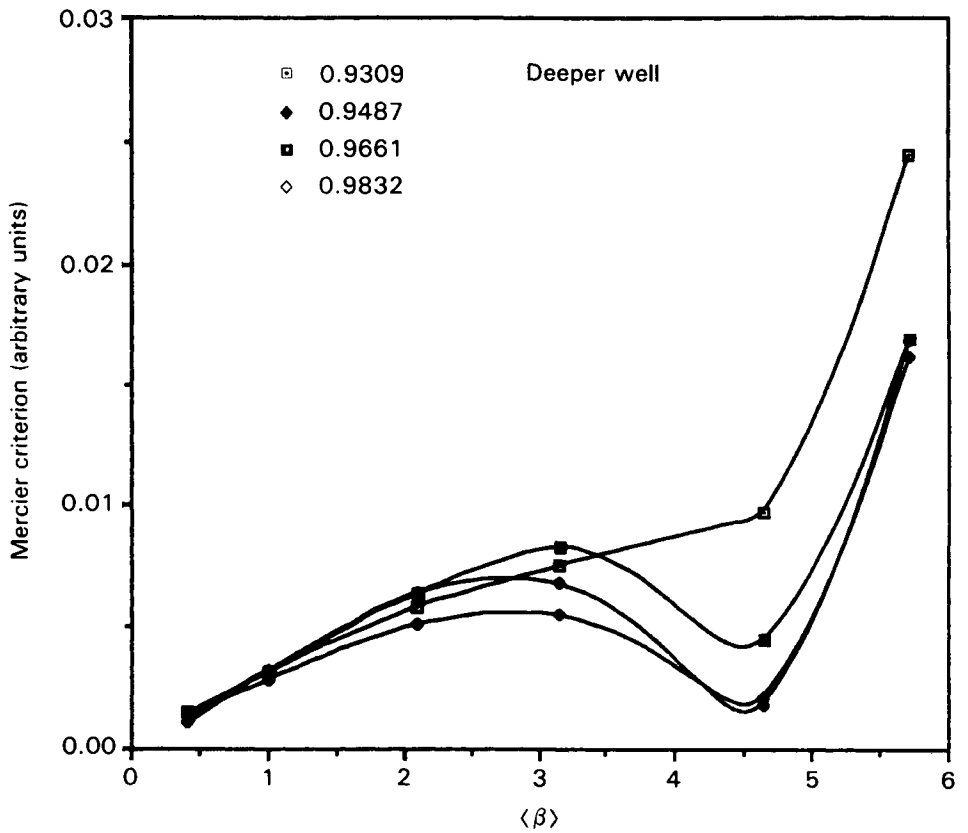

Fig. 9. The Mercier stability criterion versus $\langle\beta\rangle$ at several normalized radii for configuration B2.

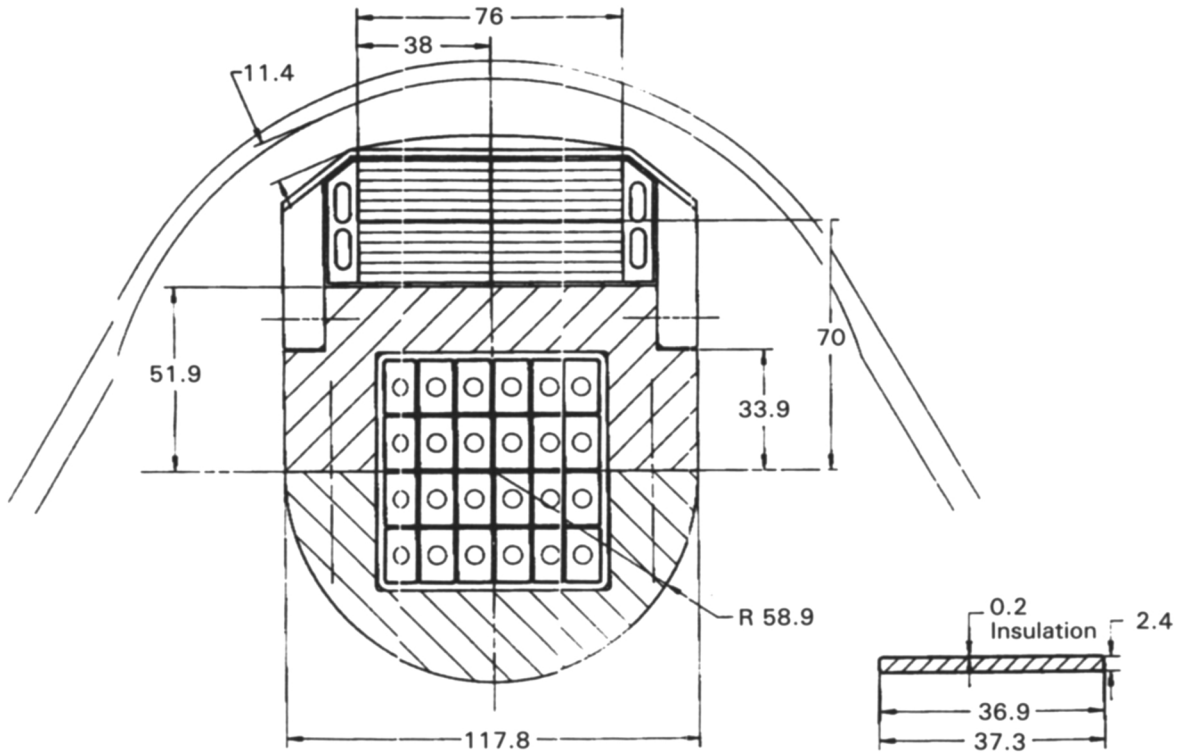

Fig. 10. Schematic of an octant of the vacuum chamber.

A high degree of access to the plasma is guaranteed through three windows per sector, located at the top, outside, and bottom of the device. There will be a total of 88 ports, as large as 15 cm wide and 50 cm long.

Coils

TF Coils

Removable coils have been chosen for TJ-II. This design, together with the vacuum chamber described above, allow the main components of the device to be built independently and assembled later in the experimental hall. They are made of copper, with a current density of ~5 kA/cm^2 and water cooling.

Hard Core Coils

The design for both the circular and the $l = 1$ helical coils are shown in Fig. 11. The copper conductors have a high density current, $j = 10$ kA/cm^2, because of the small available space. Hollow water-cooled conductors have been chosen for the circular coil. The helix will be indirectly cooled by water flowing at both sides of the winding. Calculations show that the current feeds have no influence on the vacuum magnetic surface structure.

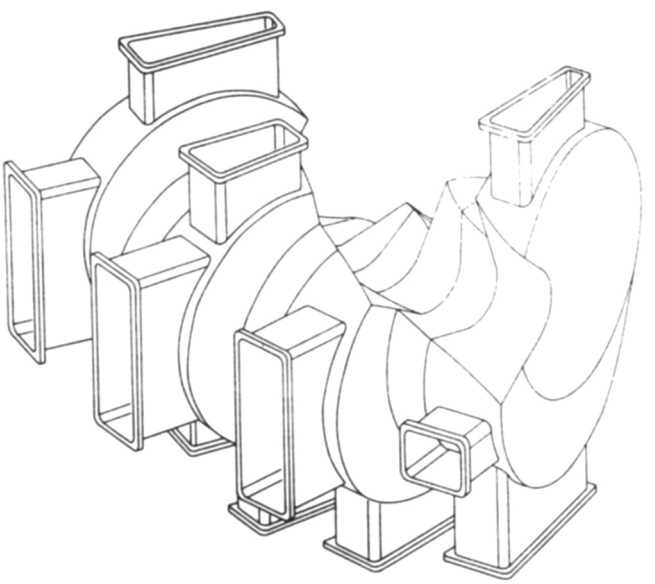

Fig. 11. Hard core coils.

SUMMARY

The TJ-II is a device to be built at Asociación EURATOM/CIEMAT to study helical-axis plasmas in a wide range of parameters. Construction of the device

is planned to start in 1990 and will take 4 yr. Design has been done in such a way that it is possible to study the most adequate configuration from the point of view of transport and stability in a first experimental program, before going into higher beta studies, by the addition of neutral beam injection, which the present design allows without major modifications.

ACKNOWLEDGMENTS

The authors want to thank the Oak Ridge National Laboratory, the IPP-EURATOM Association at Garching, and the ENEA-EURATOM Association at Frascati for their collaboration.

REFERENCES

1. A. PEREA, J. L. ALVAREZ-RIVAS, J. BOTIJA, J. R. CEPERO et al., "Physics Issues in the Design of TJ-II," *Proc. 12th European Conf. Controlled Fusion and Plasma Physics*, Budapest, Hungary, September 2-6, 1985, Europhysics Conference Abstract Series 9F, Part I, p. 433, European Physical Society (1985).

2. T. C. HENDER, J. L. CANTRELL, J. H. HARRIS, B. A. CARRERAS, V. E. LYNCH, J. F. LYON, J. A. FABREGAS, J. GUASP, A. LOPEZ-FRAGUAS, and A. P. NAVARRO, "Studies of a Flexible Heliac Configuration," *Fusion Technol.*, **13**, 521 (1988).

3. S. YOSHIKAWA, "Design of a Helical Axis Stellarator," *Nucl. Fusion*, **23**, 667 (1984).

4. T. C. HENDER, B. A. CARRERAS, and V. E. LYNCH, "Heliac Equilibria," *Nucl. Fusion*, **27**, 2161 (1987).

5. D. B. BATCHELOR and R. C. GOLDFINGER, "RAYS: A Geometrical Optics Code for EBT," ORNL/TM-6844, Oak Ridge National Laboratory (1982).

6. C. ALEJALDRE, "Influence of a Superthermal Tail upon ECRH in the TJ-II Flexible Heliac: A Theoretical Study," *Nucl. Fusion*, **28**, 849 (1988).

7. V. KRIVENSKI, I. FIDONE, G. GIRUZZI, R. L. MEYER, and L. Z. ZIEBELL, "Power Dependence of Electron Cyclotron Wave Damping in Tokamak Plasmas," *Phys. Fluids*, **30**, 438 (1987).

8. R. H. FOWLER, J. A. ROME, and J. F. LYON, "Monte Carlo Studies of Transport in Stellarators," *Phys. Fluids*, **28**, 851 (1981).

9. W. LOTZ and J. NÜRENBERG, "Monte Carlo Computations of Neoclassical Transport," *Phys. Fluids*, **31**, 2984 (1988).

10. A. VARIAS, C. ALEJALDRE, and A. L. FRAGUAS, "Stability Studies for TJ-II," *Proc. 1989 IAEA Workshop on Stellarators*, Oak Ridge, Tennessee, April 10-14, 1989 (to be published).

11. S. P. HIRSHMAN, W. I. van RIJ, and P. MERKEL, "Three-Dimensional Free Boundary Calculations Using a Spectral Green's Function Method," *Comp. Phys. Comm.*, **39**, 546 (1989).